Resource Allocation and Rate Gains in Practical Full-Duplex Systems

Jelena Marašević[1], Jin Zhou[1], Harish Krishnaswamy[1], Yuan Zhong[2], Gil Zussman[1]
[1]Electrical Engineering Dept., [2]Industrial Engineering and Operations Research Dept.
Columbia University
New York, NY, 10027, USA
{jelena@ee., jz2495@, harish@ee., yz2561@, gil@ee.}columbia.edu

ABSTRACT

Full-duplex communication has the potential to substantially increase the throughput in wireless networks. However, the benefits of full-duplex are still not well understood. In this paper, we characterize the full-duplex rate gains in both single-channel and multi-channel use cases. For the single-channel case, we *quantify the rate gain as a function of the remaining self-interference and SNR values*. We also provide a sufficient condition under which the sum of uplink and downlink rates on a full-duplex channel is concave in the transmission power levels. Building on these results, we consider the multi-channel case. For that case, we *introduce a new realistic model of a small form-factor (e.g., smartphone) full-duplex receiver* and demonstrate its accuracy via measurements. We study the problem of jointly allocating power levels to different channels and selecting the frequency of maximum self-interference suppression, where the objective is maximizing the sum of the rates over uplink and downlink OFDM channels. We develop a *polynomial time algorithm which is nearly optimal under very mild restrictions*. To reduce the running time, we develop an efficient nearly-optimal algorithm under the high SINR approximation. Finally, we demonstrate via numerical evaluations the capacity gains in the different use cases and obtain insights into the impact of the remaining self-interference and wireless channel states on the performance.

Categories and Subject Descriptors

C.2.1 [**Computer-Communication Networks**]: Network Architecture and Design—*Wireless Communication*

Keywords

Full-Duplex; Modeling; Resource Allocation

1. INTRODUCTION

Full-duplex (FD) communication – simultaneous transmission and reception on the same frequency channel – is an emerging technology that holds great promise to substantially improve the throughput in wireless networks. The main challenge hindering the implementation of practical FD devices is high self-interference (SI) caused by signal leakage from the transmitter into the receiver circuit. The SI signal is usually many orders of magnitude higher than the desired signal at the receiver's input, requiring over 100dB of self-interference cancellation (SIC).[1]

SIGMETRICS'15, June 15–19, 2015, Portland, OR, USA.

ACM 978-1-4503-3486-0/15/06 ...$15.00.
http://dx.doi.org/10.1145/2745844.2745872.

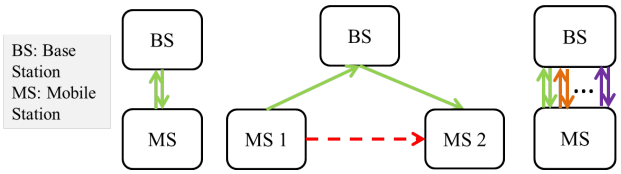

Figure 1: Some possible uses of full-duplex: (a) simultaneous uplink and downlink for one MS; (b) uplink and downlink used by two different MSs and caused inter-node interference (red dashed line), (c) simultaneous uplink and downlink over OFDM channels.

Cancelling SI is a very challenging problem. Even though ideas for different techniques of SIC were proposed over a decade ago, only recently practical circuit designs that provide sufficient SIC to be employed in Wi-Fi and cellular networks emerged (see [26] and references therein for an overview). Exciting progress has been made in the last few years by various research groups, demonstrating that a combination of SIC techniques employed both in the analog and digital domains can provide SIC levels that can support practical applications [3, 5, 8, 9, 11–14, 17–21, 24, 28, 29].

While there has been significant interest in FD from both industry and academia [2–5, 7–9, 11–15, 17–22, 24, 27–31], *the exact rate gains resulting from the use of FD are not well understood*. The first implementations of FD receivers optimistically envisioned 100% rate improvement (e.g., [5, 17]). To achieve such an increase in data rates, the FD receiver would need perfect SIC, namely to cancel SI to at least one order of magnitude below the noise floor to render it negligible. The highest reported SIC [5], however, suppresses the SI to the level of noise in the best case.

Despite this mismatch, much of the work on FD rate improvement assumes perfect SIC [4, 15, 27, 31]. While non-negligible SI has also been considered [2, 7, 22], *there are still no explicit bounds on the rate gains for given FD circuit parameters and parameters of the wireless signal*. Moreover,

[1]Namely, it is required to reduce the SI signal power by 10^{10} times.

from a modeling perspective, the frequency selectivity of SIC has not been considered in any analytical work. This is *an important feature that is inherent in conventional compact implementations of an FD receiver, such as that found in small-form factor mobile devices (e.g., smartphones and tablets)*, where frequency selectivity is mainly a consequence of the cancellation in the RF domain.[2]

Hence, *the main contribution of this paper is a thorough analytical study of rate gains from FD under non-negligible SI.* We consider both *single-channel and multi-channel orthogonal frequency division multiplexing (OFDM) scenarios.* For the multi-channel case, *we develop a new model for frequency-selective SIC in small-form factor receivers.* Our results provide explicit guarantees on the rate gains of FD, as a function of receivers' signal-to-noise ratios (SNRs) and SIC profile. Our analysis provides several insights into the structure of the sum of rates under FD, which we believe will be useful for future work on FD scheduling and MAC layer algorithm design.

Specifically, we consider three different use cases of FD, as illustrated in Fig. 1: (i) a single channel bidirectional link, where one mobile station (MS) communicates with the base station (BS) both on the uplink and on the downlink (Fig. 1(a)); (ii) two single channel unidirectional links, where one MS communicates with the BS on the uplink, while another MS communicates with the BS on the downlink (Fig. 1(b)); and (iii) a multi-channel bidirectional link, where one MS communicates with the BS over multiple OFDM channels, both on the uplink and on the downlink (Fig. 1(c)).

For SI, we consider two different models. For the BS in all use cases and the MS in use case (i), we model the remaining SI after cancellation as a constant fraction of the transmitted signal. Such design is possible for devices that do not require a very small form factor (e.g., base stations), and was demonstrated in [5].

In the multi-channel case, we rely on the characteristics of radio-frequency integrated circuit (RFIC) receivers that we recently designed [32, 34] and *develop a frequency selective model for the remaining SI in a small form-factor device.* We demonstrate the accuracy of the developed model via measurements with our receivers [32, 34].

We note that a frequency-selective profile of SIC that we model is inherent to RF cancellers with flat amplitude and phase response (see Section 3). While a mixed-signal SIC architecture [28] does not necessarily have flat amplitude and phase response, we do not consider this architecture because it requires a separate up-conversion path which introduces its own noise and distortion, limiting the resultant RF SIC.

We primarily focus on the problem of maximizing the sum of uplink and downlink rates under FD (for brevity, in the rest of the paper we refer to the sum of uplink and downlink rates as the sum rate). This problem, in general, is neither concave nor convex in the transmission power levels, since the remaining SI after cancellation often depends on the transmission power level. Due to the lack of good problem structure, existing analytical results (see e.g., [2, 7, 22]) are often restricted to specialized settings. Yet, we obtain several analytical results on the FD rate gains, often under mild restrictions, by examining closely the structural properties of the sum rate function.

[2]See our recent work [32, 34] and Section 3 for more details.

In the single-channel cases, we prove that if any rate gain can be achieved from FD, then the gain is maximized by setting the transmission power levels to their respective maximum values. This result is somewhat surprising because of the lack of good structural properties of the sum rate function. We then derive a sufficient condition under which the sum rate is concave in both transmission power levels, and show that when this condition is not satisfied, one cannot gain more than 1b/s/Hz (additively) from FD as compared to time-division duplex (TDD). We note that although the model for the remaining SI in the single channel case is relatively simple, it nonetheless captures the main characteristics of the FD sum rate, with some results extending to the multi-channel setting.

In the multi-channel case, we use the frequency-selective SI model for the MS receiver, and study the problem of transmission power allocation over OFDM channels and frequency selection, where the objective is to maximize the sum of the rates over uplink and downlink OFDM channels (in this case, frequency refers to the frequency of maximum SIC of the SI canceller). Although in general it is hard to find an optimal solution to this problem, we develop a nearly optimal algorithm under two mild technical conditions. One condition ensures that the sum rate is concave in transmission power levels. This restriction is mild, since we prove that when it does not hold, the possible gains from FD are small. Another condition imposes bounds on the magnitude of the first derivative of the sum rate in terms of maximum SIC frequency, and can be easily satisfied in an OFDM system with a large number of channels.

Although the algorithm is nearly optimal and has polynomial time complexity, its running time is relatively high. Therefore, we consider a high SINR approximation of the sum rate, and derive fixed optimal power allocation and maximum SIC frequency setting that maximizes the sum rate up to an additive ϵ in time $O(K \log(1/\epsilon))$, for any given ϵ, where K is the number of channels.

Finally, we note that throughout the paper, we provide numerical results that quantify the rate gains in various use cases and illustrate the impact of different parameters on these gains. For example, for the multi-channel case, we evaluate the rate gains using measured SI of our RFIC receiver [32, 34]. We use algorithms for the general SINR regime and for the high SINR regime, and demonstrate that for rate gains of over 50%, the outputs of the two algorithms match closely.

The rest of the paper is organized as follows. Section 2 reviews related work and Section 3 outlines the challenges in implementing FD receivers. Section 4 introduces the new model for a small form factor FD receiver, and the model for the various use cases. Section 5 provides analysis and numerical evaluation for the sum rate maximization on a single channel for use case (i). Section 6 analyzes use case (ii) and Section 7 provides analysis, algorithms, and numerical evaluation for use case (iii). We conclude in Section 8. Due to space constraints, some of the proofs are omitted and are instead provided in a technical report [23].

2. RELATED WORK

Possible rate gains from FD have been studied in [2, 4, 7, 15, 22, 27, 31], with much of the work [4, 15, 27, 31] focusing on perfect SIC. Unlike this body of work, we focus on rate gains from FD communication under imperfect SIC.

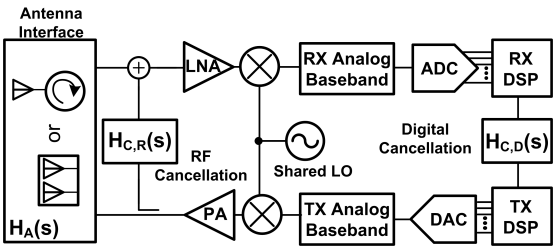

Figure 2: Block diagram of a full-duplex transceiver employing RF and digital cancellation.

Non-negligible SI has been considered in [2,7,22]. A sufficient condition for achieving positive rate gains from FD on a bidirectional link has been provided in [2], for the special case of equal SINRs on the uplink and downlink. This model takes into account the transmitter's phase noise, which is not considered in this paper. In [2], the FD capacity region is compared to the corresponding TDD capacity region, by normalizing power levels so that each station irradiates the same amount of power in both the FD and TDD regimes. In this paper, we provide explicit bounds on FD rate gains as a function of the remaining SI and uplink and downlink SNRs. Unlike [2], we bound the irradiated power of each station individually, which complies with all current Wi-Fi and cellular standards.

Power allocation over orthogonal bidirectional links was considered in [7] and [22] for MIMO and OFDM systems, respectively. The model used in [7] assumes the same amount of SIC and equal power allocation on all channels, which is a less general model than the one that we consider.

A more detailed model with different SIC over OFDM channels was considered in [22]. The model used in [22] does not consider dependence of SIC in terms of canceller frequency (although, unlike our work, it takes into account the transmitter's phase noise). Similar to [2], [22] compares the FD and TDD capacity regions of a bidirectional link by assuming equal irradiated power levels for the two duplexing methods. Optimal power allocation that maximizes one of the rates when the other is fixed is derived for equal power levels across channels, while for the general case of unequal power levels, [22] only provides a suboptimal solution.

Our work relies on structural properties of the sum rate to derive optimal power allocation and maximum SIC frequency setting that maximizes the sum rate. While the model we consider is different from [2,22], we provide a more specific characterization of achievable rate gains, and derive results that provide insights into the rate dependence on the power allocation. These results allow us to solve a very general problem of rate maximization.

3. FD IMPLEMENTATION CHALLENGES

Fig. 2 shows the block diagram of a full-duplex transceiver. There are two antenna interfaces that are typically considered for full-duplex operation: (i) an antenna pair and (ii) a circulator. The advantage of using a circulator is that it allows a single antenna to be shared between the TX and the RX. SIC must be performed in both the RF and digital domains to achieve in excess of 100dB SI suppression. The RF canceller taps a reference signal at the output of the power amplifier (PA) and performs SIC at the input of the low-noise amplifier (LNA) at the RX side [10].

(a) (b) (c)

Figure 3: (a) RFIC receiver with RF SI cancellation [32,34] and the two antenna interfaces used in our measurements: (b) an antenna pair and (c) a circulator.

Typically, 20-30dB of SIC is required from the RF, given that the antenna interface typically has a TX/RX isolation of 20-30dB [1]. Thus, an overall 50-60dB RF TX/RX isolation is achieved before digital SIC is engaged. This amount of RF TX/RX isolation is critical to alleviate the RX linearity and the analog-to-digital conversion (ADC) dynamic range requirements [10,26]. Digital cancellation further cancels the linear SI as well as the non-linear distortion products generated by the RX or the RF canceller.

A mixed-signal SIC architecture has been proposed in [28], where the digital TX signal is processed and upconverted to RF for cancellation. However, this requires a separate upconversion path which introduces its own noise and distortion. Moreover, the noise and distortion of the TX analog and RF circuits (such as the power amplifier) are not readily captured in the cancellation signal, limiting the resultant RF SIC. In addition, the dedicated up-conversion path results in area and power overhead. Because of these reasons, we are not considering this SIC architecture in this paper.

For wideband SIC, the transfer function of the canceller must closely track that of the antenna interface across frequency. However, the frequency dependence of the inherent antenna interface isolation together with selective multipath-ridden SI channels render this challenging for the RF canceller in particular. The net antenna interface isolation amplitude and phase response can vary significantly with frequency. A rapidly-varying phase response is representative of a large group delay, requiring bulky delay lines to replicate the selectivity in the RF canceller [5,10].

The fundamental challenge associated with wideband SIC at RF in a compact form-factor and/or using integrated circuits is the generation of large time delays. The amount of true time delay is linearly proportional to the dimension of the delay structure and inversely proportional to the wave velocity in the medium. To generate 1ns delay in a silicon integrated circuit, a transmission line of 15cm length is required as the relative dielectric constant of silicon oxide is 4. Therefore, a conventional integrated RF SI canceller with dimensions less than 1mm^2 will exhibit negligible delay, and *the amplitude and phase response of the canceller can be assumed to be flat with respect to frequency* when compared with antenna interface's isolation, limiting the cancellation bandwidth [26,32].

While achieving wideband RF SI cancellation using innovative RFIC techniques is an active research topic (e.g., frequency domain equalization based RF SI cancellation in [33]), in this paper we focus on compact flat amplitude- and phase-based RF cancellers, such as the one we implemented in the RFIC depicted in Fig. 3(a) [32,34].

We measured isolation amplitude and group delay response of (i) a PCB antenna pair (see Fig. 3(b)) and (ii) a commercial 2110-2170MHz miniature circulator from Skyworks [1] (see Fig. 3(c)). The results are shown in Fig. 4(a) and

$$RSI_{m,k} = (|H_A|^2 P_{m,k} + |H_{C,R}|^2 P_{m,k} - 2\sqrt{|H_A|^2 P_{m,k} |H_{C,R}|^2 P_{m,k}} \cdot \cos(\angle H_A(f_k) + \angle H_{C,R}))SIC_D^{-1}. \quad (1)$$

Fig. 4(b), respectively. The resultant TX/RX isolations using an RF canceller with flat amplitude and phase response after the antenna interfaces (i) and (ii) are shown in Fig. 4(c) and Fig. 4(d), respectively. As Fig. 4(c) and Fig. 4(d) suggest, for -60dB TX/RX isolation after RF cancellation, the bandwidths are about 4MHz and 2.5MHz, respectively.

4. MODEL

We consider three use cases of FD: (i) a bidirectional link, where one mobile station (MS) communicates with the base station (BS) both on the uplink and on the downlink (Fig. 1(a)), (ii) two unidirectional links, where one MS is communicating with the BS on the uplink, while another MS is communicating with the BS on the downlink (Fig. 1(b)), and (iii) multiple orthogonal bidirectional links (Fig. 1(c)). Note that in (ii) only the BS is operating in FD.

For the multi-channel FD (use case (iii)), we assume that the network bandwidth of size B is subdivided into K orthogonal frequency channels of width B/K each, and index the frequency channels with $k \in \{1, ..., K\}$. An example of such sub-channelization is OFDM with each frequency channel consisting of an integral number of subcarriers.

For all notation that relates to the BS, we will use b in the subscript. For the notation that relates to the MS in use cases (i) and (iii), we will use m in the subscript, while in the use case (ii) we will use m_1 and m_2 to refer to MS 1 and MS 2, respectively. Summary of the main notation is provided in Table 1.

The transmission power of a station $u \in \{b, m, m_1, m_2\}$ on channel k is denoted by $P_{u,k}$, where $k \in \{1, ..., K\}$. In use cases (i) and (ii), k is omitted from the subscript, since we consider a single channel.

4.1 Remaining SI

Single-channel FD. For single-channel FD, we assume that the remaining SI both at the BS and at an MS can be expressed as a constant fraction of the transmitted power. In particular, if the BS transmits at the power level P_b, the remaining SI is $RSI_b = g_b P_b$, where g_b is a constant determined by the hardware. Similarly, if an MS transmits at the power level P_m, its remaining SI is $RSI_m = g_m P_m$.

Multi-channel FD. We assume that the FD receiver at the BS has frequency-flat SIC profile, meaning that the remaining SI at the BS on channel k is $RSI_{b,k} = g_b P_{b,k}$, where g_b is a constant. We note that such FD receiver design is possible to implement in devices that do not require small form factor of the circuit (e.g., a BS or an access point (AP)), and has been reported in [5].

In the rest of this section, we describe the mathematical model of the remaining SI for a small form factor device (MS). We consider a compact/RFIC FD receiver with a *circulator* at the antenna interface, described in Section 3, and assume a frequency-flat amplitude and phase response of the canceller, denoted by $|H_{C,R}|$ and $\angle H_{C,R}$, respectively. The amplitude and phase response of the canceller are assumed to be programmable but constant with frequency.

For the antenna interface's TX/RX isolation, we assume a flat amplitude response $|H_A(f)| = const = |H_A|$ and a constant group delay equal to τ, so that $H_A(f) = |H_A|e^{-j2\pi f\tau}$ (recall that the measured amplitude and phase response are shown in Fig. 4(b)). For the digital SIC, denoted by SIC_D, we assume that the amount of cancellation is constant across frequency, as delay can be easily generated in the digital domain.

Let f_k denote the central frequency of the k^{th} channel, so that $f_k = f_1 + (k-1)B/K$. Then, the remaining SI after cancellation can be written as (1).

We assume a common oscillator for the TX and RX, with the phase noise of the oscillator being good enough so that it does not affect the remaining SI.

The RF canceller's settings can be programmed in the field to adjust the frequency at which peak SIC is achieved [32, 34]. With the amplitude ($|H_{C,R}|$) and the phase ($\angle H_{C,R}$) of the RF canceller set to $|H_A|$ and $-\angle H_A(f_{c_i})$, respectively, peak SIC is achieved at frequency f_c. Therefore, the total remaining SI at the MS on channel k can be written as:

$$RSI_{m,k} = 2|H_A|^2 P_{m,k}(1 - \cos(2\pi\tau(f_k - f_c)))SIC_D^{-1},$$

where τ is the group delay from the antenna interface with a typical value at the order of 1ns (which agrees with the measured group delay in Fig. 4(b)). Frequency bands used by commercial wireless systems are at most 10s of MHz wide. It follows that $2\pi\tau(f_k - f_c) << 1$, and using the standard approximation $\cos(x) \approx 1 - x^2/2$ for $x << 1$, we further get:

$$RSI_{m,k} \approx |H_A|^2 P_{m,k}(2\pi\tau)^2(f_k - f_c)^2 SIC_D^{-1}.$$

Recalling that $f_k = f_1 + (k-1)B/K = f_0 + kB/K$ for $f_0 = f_1 - B/K$, and writing f_c as $f_c = f_0 + cB/K$, for $c \in \mathbb{R}$, we can combine all the constant terms and represent the remaining SI as:

$$RSI_{m,k} = g_m P_{m,k}(k - c)^2, \quad (2)$$

where $g_m = |H_A|^2(2\pi\tau)^2(B/K)^2 SIC_D^{-1}$. Note that even though in this notation we allow c to take negative values, we will later show that in any solution that maximizes the sum rate it must be $c \in (1, K)$ (Lemma 7.3).

Fig. 4(d) shows the TX/RX isolation based on Eq. (2) and based on measurement results. The parameter g_m in Eq. (2) was determined via a least square estimation. The modeled TX/RX isolation based on Eq. (2) is also compared to the measured TX/RX isolation of the canceller with the antenna pair interface in Fig. 4(c). *As Fig. 4 shows, our model of the remaining SI closely matches the remaining SI that we measured with the RFIC FD receiver presented in* [32, 34].

4.2 Sum Rate

The total transmitted power of each station is assumed to be bounded as follows. In use cases (i) and (ii): $P_b \leq \overline{P_b}$, and each $P_m, P_{m_1}, P_{m_2} \leq \overline{P_m}$. In use case (iii): $\sum_{k=1}^{K} P_{u,k} \leq \overline{P_u}$, where $u \in \{b, m\}$, $\overline{P_u} > 0$. The channel gain from station u to station v on channel k is denoted by $h_{uv,k}$ in use case (iii) and by h_{uv} in use cases (i) and (ii). The noise level at station u is assumed to be equal on each channel and is denoted by N_u.

For the signal transmitted from u to v, where $u, v \in \{b, m, m_1, m_2\}$, $u \neq v$, and either $u = b$ or $v = b$, we let $\gamma_{uv,k} = \frac{h_{uv,k}}{N_v}$ denote signal to noise ratio (SNR) at v on channel k. Similarly as before, in use cases (i) and (ii), index k is omitted from the notation. In the use case (ii),

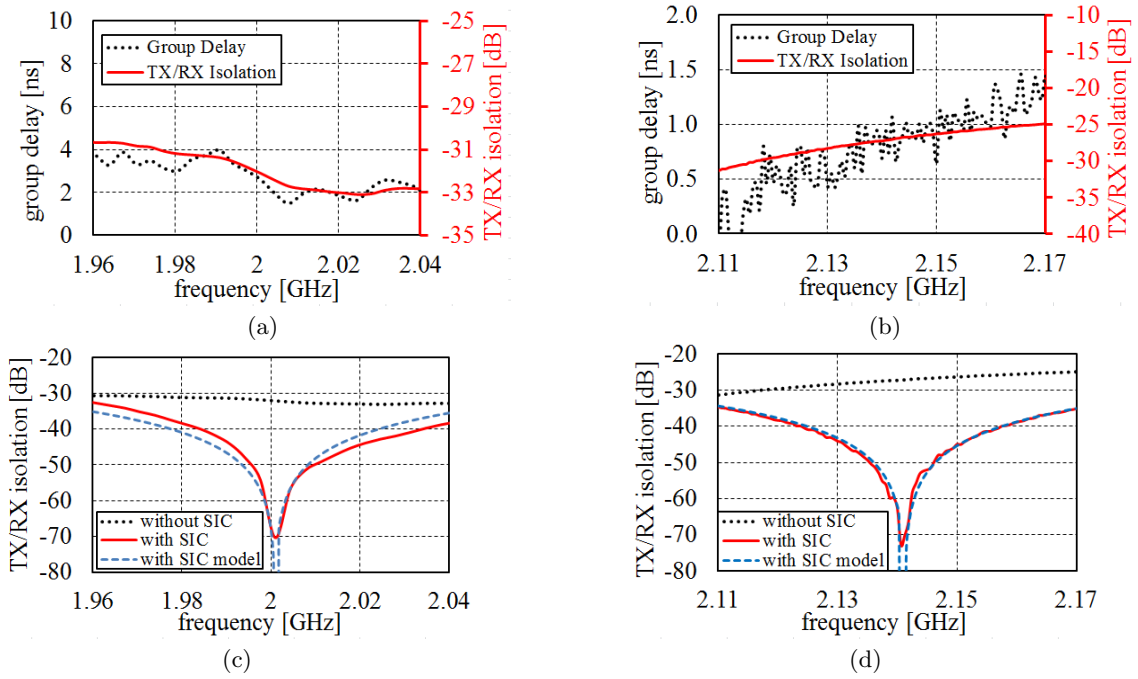

Figure 4: Measured isolation amplitude and group delay of (a) a PCB antenna pair and (b) a commercial 2110-2170 MHz miniature circulator from Skyworks [1], and the resultant TX/RX isolation using the integrated RF canceller with flat amplitude and phase response from [32, 34] with (c) the antenna pair and (d) the circulator compared to the modeled SIC.

Table 1: Nomenclature.

m	Subscript notation for an MS
b	Subscript notation for the BS
K	Total number of OFDM channels
k	Channel index, $k \in \{1, ..., K\}$
u, v	Station indexes, $u, v \in \{b, m, m_1, m_2\}$
$P_{u,k}$	Transmission power of station u on channel k
$\overline{P_u}$	Maximum total power: $\sum_{k=1}^{K} P_{u,k} \leq \overline{P_u}$
g_b	Remaining SI at the BS per unit transmitted power
c	Position of the maximum SIC frequency, $c \in \mathbb{R}$
g_m	Remaining SI at an MS per unit transmitted power for $K = 1$; Remaining SI at an MS per unit transmitted power at unit distance from the maximum SIC frequency for $K > 1$
$h_{uv,k}$	Wireless channel gain for signal from u to v on channel k, for $u \neq v$
N_u	Thermal noise at station u
$\gamma_{uv,k}$	SNR of signal from u to v on channel k, where $u \neq v$
$\gamma_{uu,k}$	XINR at station u, channel k
$\gamma_{uv,k}^{\max}$	$\gamma_{uv,k}$ for $P_u = \overline{P_u}$
r_k	Total rate on channel k
r	Sum rate: $r = \sum_{k=1}^{K} r_k$
$r_{\text{TDD}}^{\max}$	Maximum TDD rate.

$\gamma_{m_1 m_2}$ denotes the (inter-node-)interference to noise ratio (INR). Self-interference to noise ratio (XINR) at the BS is denoted by $\gamma_{bb} = \frac{g_b P_b}{N_b}$ in use cases (i) and (ii), and by $\gamma_{bb,k} = \frac{g_b P_{b,k}}{N_b}$ in use case (iii). XINR at the MS is denoted by $\gamma_{mm} = \frac{g_m P_m}{N_m}$ and $\gamma_{mm,k} = \frac{g_m (k-c)^2 P_{m,k}}{N_m}$ in use cases (i) and (iii), respectively.

We use Shannon's capacity formula for spectral efficiency, and let log(.) denote the base 2 logarithm, ln(.) denote the natural logarithm. We use the terms "spectral efficiency" and "rate" interchangeably, as the spectral efficiency on a channel is the rate on that channel normalized by B/K.[3]

In use case (i), the sum rate on the channel is given as:

$$r = \log\left(1 + \frac{\gamma_{mb}}{1 + \gamma_{bb}}\right) + \log\left(1 + \frac{\gamma_{bm}}{1 + \gamma_{mm}}\right). \quad (3)$$

Observe that $\frac{\gamma_{mb}}{1+\gamma_{bb}}$ and $\frac{\gamma_{bm}}{1+\gamma_{mm}}$ are signal to interference-plus-noise ratios (SINRs) on the uplink and downlink, respectively. We will refer to $r_m = \log\left(1 + \frac{\gamma_{mb}}{1+\gamma_{bb}}\right)$ as the uplink rate and $r_b = \log\left(1 + \frac{\gamma_{bm}}{1+\gamma_{mm}}\right)$ as the downlink rate.

Similarly as for (i), the sum rate for use case (ii) is:

$$r = \log\left(1 + \frac{\gamma_{m_1 b}}{1 + \gamma_{bb}}\right) + \log\left(1 + \frac{\gamma_{bm_2}}{1 + \gamma_{m_1 m_2}}\right). \quad (4)$$

Finally, in use case (iii), the rate on channel k is given as:

$$r_k = \log\left(1 + \frac{\gamma_{mb,k}}{1 + \gamma_{bb,k}}\right) + \log\left(1 + \frac{\gamma_{bm,k}}{1 + \gamma_{mm,k}}\right), \quad (5)$$

while the sum rate (on all channels) is $r = \sum_{k=1}^{K} r_k$.

The objective in all problems considered in this paper is to maximize r subject to the upper bound on total transmitted power and non-negativity constraints. In use cases (i) and (ii), the variables are P_b and P_m, while in the use case (iii), the variables are c, $P_{b,k}$, and $P_{m,k}$, for $k \in \{1, ..., K\}$.

For the purpose of comparison to TDD systems, we will sometimes also consider TDD rates. A pair of uplink and downlink TDD rates $r_{\text{TDD},m}$ and $r_{\text{TDD},b}$ is feasible if there exist $a_m, a_b \geq 0$ such that $a_m + a_b \leq 1$ and $r_{\text{TDD},m} =$

[3]Note that this is true both in single-channel and multi-channel cases, since in the single-channel case $K = 1$.

$a_m \log(1+\gamma_{mb})$, $r_{\mathrm{TDD},b} = a_b \log(1+\gamma_{bm})$. We let $r^{\max}_{\mathrm{TDD}}$ denote the maximum of the sum $r_{\mathrm{TDD},m} + r_{\mathrm{TDD},b}$.

5. A BIDIRECTIONAL FD LINK

In this section, we derive general properties of the sum rate function for use case (i) (Fig. 1(a)).

First, we show that if it is possible for the FD sum rate to exceed the maximum TDD rate, it is always optimal for the MS and the BS to transmit at their maximum respective power levels (Lemma 5.1). This result is somewhat surprising, because in general, the FD sum rate function does not have good structural properties, i.e., it need not be convex or concave in the transmission power variables.

Building upon this insight, we quantify the FD rate gains by comparing the FD sum rate to corresponding TDD rates (Section 5.2). More specifically, we define a metric that characterizes by how much the FD capacity region extends the corresponding TDD capacity region, and provide a sufficient condition on the system parameters for rate gains to hold.

Finally, we establish a sufficient condition for the FD sum rate function to be concave in transmission power levels (Section 5.3). This condition imposes very mild restrictions on the XINRs at the BS and the MS. Moreover, the established condition extends to the multi-channel scenario (use case (iii)), where it plays a crucial role in deriving a nearly-optimal algorithm for the sum rate maximization (Section 7.2.1).

5.1 Power Allocation

LEMMA 5.1. *If there exists an FD sum rate r that is higher than the maximum TDD rate, then r is maximized for $P_m = \overline{P_m}$, $P_b = \overline{P_b}$.*

PROOF. From (3), the sum rate can be written as:

$$r = \log\left(1+\frac{h_{mb}P_m}{N_b+g_bP_b}\right)+\log\left(1+\frac{h_{bm}P_b}{N_m+g_mP_m}\right)$$

Taking partial derivatives of r directly does not provide conclusive information about the optimal power levels. Instead, we write r as an increasing function of another function that is easier to analyze. Specifically:

$$\begin{aligned} r &= \log\left(\left(1+\frac{h_{mb}P_m}{N_b+g_bP_b}\right)\cdot\left(1+\frac{h_{bm}P_b}{N_m+g_mP_m}\right)\right) \\ &= \log(1+\gamma), \quad \text{where} \\ \gamma &= \frac{h_{mb}P_m}{N_b+g_bP_b}+\frac{h_{bm}P_b}{N_m+g_mP_m}+\frac{h_{mb}P_m}{N_b+g_bP_b}\cdot\frac{h_{bm}P_b}{N_m+g_mP_m}. \end{aligned}$$

Since r is strictly increasing in γ, to maximize r it suffices to determine P_m, P_b that maximize γ.

The first and the second partial derivative of γ with respect to P_m are:

$$\frac{\partial\gamma}{\partial P_m} = \frac{h_{mb}}{N_b+g_bP_b}+\frac{h_{bm}P_b}{(N_m+g_mP_m)^2}\left(\frac{h_{mb}N_m}{N_b+g_bP_b}-g_m\right), \tag{6}$$

$$\frac{\partial^2\gamma}{\partial {P_m}^2} = -2\frac{h_{bm}P_bg_m}{(N_m+g_mP_m)^3}\left(\frac{h_{mb}N_m}{N_b+g_bP_b}-g_m\right). \tag{7}$$

From (6) and (7):

1. If $\frac{h_{mb}N_m}{N_b+g_bP_b}-g_m \geq 0$, then $\frac{\partial^2\gamma}{\partial {P_m}^2} \leq 0$ and $\frac{\partial\gamma}{\partial P_m} > 0$, which implies that γ is concave and strictly increasing in P_m, and therefore maximized for $P_m = \overline{P_m}$.

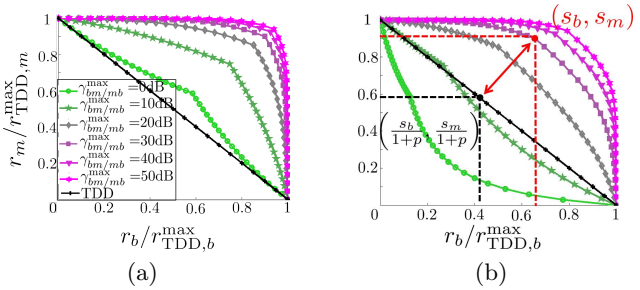

(a) (b)

Figure 5: TDD and FD capacity regions, and FD extension. The capacity region is plotted for equal maximum SNRs: $\gamma^{\max}_{mb} = \gamma^{\max}_{bm} \equiv \gamma^{\max}_{bm/mb}$ and two cases of maximum XINRs: (a) $\gamma^{\max}_{bb} = 1$, $\gamma^{\max}_{mm} = 1$ and (b) $\gamma^{\max}_{bb} = 1$, $\gamma^{\max}_{mm} = 10$.

2. If $\frac{h_{mb}N_m}{N_b+g_bP_b}-g_m < 0$, then $\frac{\partial^2\gamma}{\partial {P_m}^2} > 0$, which means that γ is strictly convex in P_m. Therefore, γ is maximized at either $P_m = 0$ or $P_m = \overline{P_m}$. Note that if $P_m = 0$, there is no signal on uplink, in which case FD rate equals the maximum TDD uplink rate.

A similar results follows for P_b by taking the first and the second partial derivative of γ with respect to P_b. □

5.2 Mapping Gain over SINR Regions

In this section we quantify the FD rate gains by comparing the FD capacity region to the corresponding TDD capacity region. Let $r_b = \log(1+\frac{\gamma_{bm}}{1+\gamma_{mm}})$, $r_m = \log(1+\frac{\gamma_{mb}}{1+\gamma_{bb}})$ denote downlink and uplink rates, respectively and let $r^{\max}_{\mathrm{TDD},b} = \log(1+\gamma^{\max}_{bm})$, $r^{\max}_{\mathrm{TDD},m} = \log(1+\gamma^{\max}_{mb})$ denote the maximum TDD rates. The FD capacity region is the set of all points (r_b, r_m) such that $P_m \in [0, \overline{P_m}]$, $P_b \in [0, \overline{P_b}]$, while the TDD capacity region is the convex hull of the points $(0,0)$, $(r^{\max}_{\mathrm{TDD},b}, 0)$, and $(0, r^{\max}_{\mathrm{TDD},m})$.

We also let $s_b = \log(1+\frac{\gamma^{\max}_{bm}}{1+\gamma^{\max}_{mm}})$ and $s_m = \log(1+\frac{\gamma^{\max}_{mb}}{1+\gamma^{\max}_{bb}})$ be the FD downlink and uplink rates when both stations transmit at their maximum power levels $\overline{P_b}, \overline{P_m}$.

Fig. 5 shows FD and TDD capacity regions for symmetric maximum SNRs $\gamma^{\max}_{mb} = \gamma^{\max}_{bm}$ and two cases of maximum XINRs: $\gamma^{\max}_{bb} = \gamma^{\max}_{mm} = 1$ and $\gamma^{\max}_{bb} = 1$, $\gamma^{\max}_{mm} = 10$. Here, the axes are normalized by $r^{\max}_{\mathrm{TDD},b}$ and $r^{\max}_{\mathrm{TDD},m}$, respectively. Note that FD capacity regions are not necessarily convex (e.g., Fig. 5(b) for $\gamma^{\max}_{bm/mb} = 0$dB and $\gamma^{\max}_{bm/mb} = 10$dB).

Lemma 5.1 states that the maximizer of the FD sum rate is either $(r^{\max}_{\mathrm{TDD},b}, 0)$, $(0, r^{\max}_{\mathrm{TDD},m})$ or (s_b, s_m). In particular, to see whether FD operation increases the sum rate, it suffices to check whether $s_b + s_m > \max\{r^{\max}_{\mathrm{TDD},b}, r^{\max}_{\mathrm{TDD},m}\}$. This motivates us to focus on the pair (s_b, s_m) when considering by how much the FD capacity region extends the corresponding TDD capacity region. We introduce the following definition (see Fig. 5(b) for a geometric interpretation).

Definition 1. FD extends the corresponding TDD capacity region by $p \cdot 100\%$ if $p \geq 0$ is the smallest number for which $\frac{s_b}{1+p}, \frac{s_m}{1+p}$ is inside the TDD capacity region.

The following lemma provides a necessary and sufficient condition for the capacity region extension of $p \cdot 100\%$.

LEMMA 5.2. *FD extends the TDD capacity region by $p \cdot 100\%$, where $p \geq 0$, if and only if:*

$$\frac{\log\left(1+\frac{\gamma^{\max}_{bm}}{1+\gamma^{\max}_{mm}}\right)}{\log(1+\gamma^{\max}_{bm})}+\frac{\log\left(1+\frac{\gamma^{\max}_{mb}}{1+\gamma^{\max}_{bb}}\right)}{\log(1+\gamma^{\max}_{mb})} = 1+p. \tag{8}$$

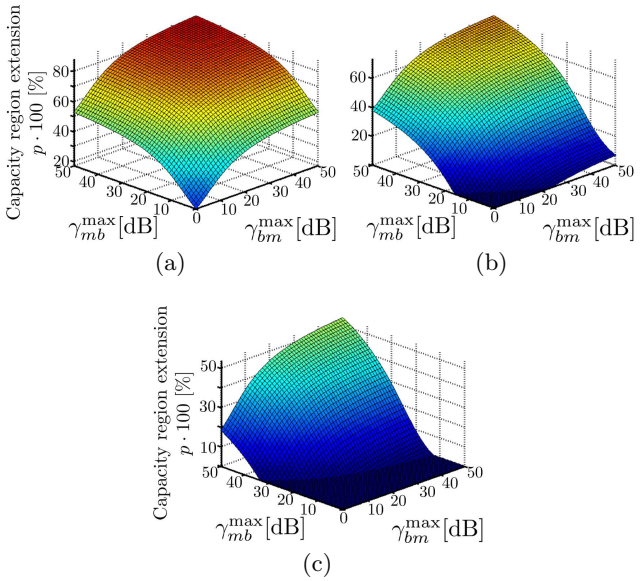

Figure 6: TDD capacity region extension due to FD as a function of SNRs for (a) $\gamma_{bb}^{\max} = 1$, $\gamma_{mm}^{\max} = 1$, (b) $\gamma_{bb}^{\max} = 1$, $\gamma_{mm}^{\max} = 10$, and (c) $\gamma_{bb}^{\max} = 1$, $\gamma_{mm}^{\max} = 100$.

Proof Sketch. The proof is based on the fact that since p is the smallest number for which the point $(\frac{s_b}{1+p}, \frac{s_m}{1+p})$ is in the TDD capacity region, $(\frac{s_b}{1+p}, \frac{s_m}{1+p})$ must lie on the line connecting $r_{\mathrm{TDD},b}^{\max}$ and $r_{\mathrm{TDD},m}^{\max}$ (Fig. 5(b)), and therefore: $\frac{s_m}{1+p} = r_{\mathrm{TDD},m}^{\max} - \frac{r_{\mathrm{TDD},m}^{\max}}{r_{\mathrm{TDD},b}^{\max}} \frac{s_b}{1+p}$, which is equivalent to $\frac{\log\left(1+\frac{\gamma_{bm}^{\max}}{1+\gamma_{mm}^{\max}}\right)}{\log(1+\gamma_{bm}^{\max})} + \frac{\log\left(1+\frac{\gamma_{mb}^{\max}}{1+\gamma_{bb}^{\max}}\right)}{\log(1+\gamma_{mb}^{\max})} = 1+p$. □

Fig. 6 shows the TDD capacity region extension due to FD operation, as a function of received signals' SNR, for BS FD receiver that cancels SI to the noise level and MS FD receiver that cancels SI to (i) the noise level (Fig. 6(a)), (ii) one order of magnitude above noise (Fig. 6(b)), and (iii) two orders of magnitude above noise (Fig. 6(c)). Somewhat surprisingly, even in the case when the MS cancels SI to two orders of magnitude above noise, capacity region extension can be as high as 50% for sufficiently high SNRs (Fig. 6(c)).

5.3 Sum Rate Concavity

In this section, we establish a sufficient condition for the sum rate to be (strictly) concave, and increasing in P_m and in P_b (Condition 5.3). We also show that when the condition fails, using FD does not provide appreciable rate gains, as compared to the maximum rate achievable by TDD operation.

Condition 5.3. $\gamma_{mm} \leq \frac{\gamma_{mb}}{1+\gamma_{bb}}$ *and* $\gamma_{bb} \leq \frac{\gamma_{bm}}{1+\gamma_{mm}}$.

Proposition 5.4. *If* $\gamma_{mm} \leq \frac{\gamma_{mb}}{1+\gamma_{bb}}$, *the sum rate* r *is strictly concave and strictly increasing in* P_m. *Similarly, if* $\gamma_{bb} \leq \frac{\gamma_{bm}}{1+\gamma_{mm}}$, r *is strictly concave and strictly increasing in* P_b. *Thus, when Condition 5.3 holds,* r *is strictly concave and strictly increasing both in* P_m *and in* P_b. *Furthermore, when Condition 5.3 does not hold,* $r - r_{TDD}^{\max} < 1b/s/Hz$.

Proof. From the proof of Lemma 5.1, we can express r as $r = \log(1+\gamma)$, where γ is strictly increasing and concave in P_m whenever

$$\frac{h_{mb}N_m}{N_b + g_b P_b} - g_m \geq 0. \tag{9}$$

Multiplying both sides of (9) by $\frac{P_m}{N_m}$ and reordering terms:

$$\frac{h_{mb}P_m}{N_b + g_b P_b} \geq \frac{g_m P_m}{N_m} \quad \Leftrightarrow \quad \gamma_{mm} \leq \frac{\gamma_{mb}}{1+\gamma_{bb}}.$$

Whenever (9), or equivalently, the inequality $\gamma_{mm} \leq \frac{\gamma_{mb}}{1+\gamma_{bb}}$, holds, since $\gamma > 0$, $\frac{\partial\gamma}{\partial P_m} > 0$, $\frac{\partial^2\gamma}{\partial {P_m}^2} \leq 0$:

$$\frac{\partial r}{\partial P_m} = \frac{1}{1+\gamma} \cdot \frac{\partial \gamma}{\partial P_m} > 0, \text{ and,}$$
$$\frac{\partial^2 r}{\partial {P_m}^2} = -\frac{1}{(1+\gamma)^2} \cdot \left(\frac{\partial\gamma}{\partial P_m}\right)^2 + \frac{1}{1+\gamma} \cdot \frac{\partial^2\gamma}{\partial {P_m}^2} < 0,$$

and therefore r is strictly increasing and strictly concave in P_m. Similarly, whenever $\gamma_{bb} \leq \frac{\gamma_{bm}}{1+\gamma_{mm}}$, r is strictly increasing and strictly concave in P_b.

Now suppose that Condition 5.3 does not hold. Then, either $\gamma_{mm} > \frac{\gamma_{mb}}{1+\gamma_{bb}}$ or $\gamma_{bb} > \frac{\gamma_{bm}}{1+\gamma_{mm}}$. Suppose that $\gamma_{mm} > \frac{\gamma_{mb}}{1+\gamma_{bb}}$. Then:

$$\begin{aligned} r &= \log\left(1+\frac{\gamma_{mb}}{1+\gamma_{bb}}\right) + \log\left(1+\frac{\gamma_{bm}}{1+\gamma_{mm}}\right) \\ &< \log\left(1+\frac{\gamma_{mb}}{1+\gamma_{bb}}\right) + \log\left(1+\frac{\gamma_{bm}}{1+\frac{\gamma_{mb}}{1+\gamma_{bb}}}\right) \\ &= \log\left(1+\gamma_{bm}+\frac{\gamma_{mb}}{1+\gamma_{bb}}\right) \\ &= \log\left(2\cdot\left(1+\frac{1}{2}\left(\gamma_{bm}+\frac{\gamma_{mb}}{1+\gamma_{bb}}-1\right)\right)\right) \\ &= 1\text{b/s/Hz} + \log\left(1+\frac{1}{2}\left(\gamma_{bm}+\frac{\gamma_{mb}}{1+\gamma_{bb}}-1\right)\right). \end{aligned}$$

Since $\frac{1}{2}\left(\gamma_{bm}+\frac{\gamma_{mb}}{1+\gamma_{bb}}-1\right) < \max\{\gamma_{mb}, \gamma_{bm}\}$, it follows that $r < 1\text{b/s/Hz} + r_{\mathrm{TDD}}^{\max}$, which completes the proof for $\gamma_{mm} > \frac{\gamma_{mb}}{1+\gamma_{bb}}$. The proof for the case $\gamma_{bb} > \frac{\gamma_{bm}}{1+\gamma_{mm}}$ follows the same line of argument and is omitted for brevity. □

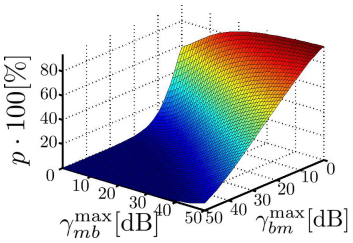

Figure 7: Capacity region extension when Condition 5.3 is not satisfied. Non-negligible gains are possible only when uplink SNR is at least an order of magnitude higher than the downlink SNR, a case that is irrelevant in practice.

When Condition 5.3 does not hold, the bound $r - r_{\mathrm{TDD}}^{\max} < 1\text{b/s/Hz}$ limits the additive increase in FD rate. However, it does not bound the FD capacity region extension. Therefore, we plot an upper bound on the FD capacity region extension in Fig. 7 for a perfect SIC at the BS ($\gamma_{bb} = 0$) and $\gamma_{mm} = \frac{\gamma_{mb}}{1+\gamma_{bb}} = \gamma_{mb}$. As Fig. 7 shows, to have non-negligible capacity region extension, the uplink SNR γ_{mb} should be higher than the downlink SNR γ_{bm}. This is rarely

the case in practice, since in cellular and Wi-Fi networks typically the opposite holds, i.e., $\gamma_{bm} > \gamma_{mb}$, due to better antenna gain and higher transmission power at the BS/AP.

Note that the condition for concavity in P_b, $\gamma_{bb} \leq \frac{\gamma_{bm}}{1+\gamma_{mm}}$, is relatively simple to satisfy, since in practice it is possible to achieve $\gamma_{bb} = 1$ [5], and the condition is satisfied for downlink SINR (SINR at the MS) $\geq$ 0dB.

6. TWO UNIDIRECTIONAL LINKS

Much of the analysis for use case (i) (Section 5) extends to use case (ii) (Fig. 1(b)), due to the similarity between the sum rate as a function of transmission power levels for these two use cases (see Eqs. (3) and (4)). However, there are also important differences. First, the interfering signal at MS 2 in use case (ii), unlike the self-interfering signal at the MS in the bidirectional link case, is not known at the receiver, and therefore, cannot be cancelled (unless an additional channel is used, which we do not consider). Second, in use case (ii), the channel gains between MSs cannot take arbitrary values. This is because the channel gains typically conform to a path loss model of propagation, where the SNR depends on distances between MSs, which in turn need to satisfy the triangle inequality. The following two lemmas are similar to Lemmas 5.1 and 5.2. We state them without proofs.

LEMMA 6.1. *If there exists an FD sum rate that is higher than the maximum TDD rate, then the FD sum rate is maximized at $P_{m_1} = \overline{P_m}$ for MS 1, and $P_b = \overline{P_b}$ for the BS.*

LEMMA 6.2. *FD extends the TDD capacity region by $p \cdot 100\%$ if and only if:*

$$\frac{\log\left(1+\frac{\gamma_{bm_2}^{\max}}{1+\gamma_{m_1m_2}^{\max}}\right)}{\log(1+\gamma_{bm_2}^{\max})} + \frac{\log\left(1+\frac{\gamma_{m_1b}^{\max}}{1+\gamma_{bb}^{\max}}\right)}{\log(1+\gamma_{m_1b}^{\max})} = 1+p. \quad (10)$$

In a path loss model of propagation, the wireless channel gain between two stations is a function of the distance between the stations: $h_{uv} = \left(\frac{L}{d_{uv}}\right)^{\eta}$, where $u, v \in \{b, m_1, m_2\}$, $u \neq v$, η is the path loss exponent, and L is a constant. Therefore, since distances d_{m_1b}, d_{bm_2}, and $d_{m_1m_2}$ need to satisfy the triangle inequality, SNRs γ_{m_1b}, γ_{bm_2} and INR $\gamma_{m_1m_2}$ cannot take arbitrary values.

To evaluate rate gains in use case (ii), we consider path loss exponents from the set $\{2, 3, 4\}$, since typical range for the path loss exponent is between 2 and 4 [25]. We assume fixed maximum power levels at the BS and the MS 1, equal noise levels N at the BS and the MS 2, and we vary SNRs and the INR as the function of distance, as follows:

$$\gamma_{m_1b} = \frac{h_{m_1b}\overline{P_{m_1}}}{N} = \frac{h_{m_1b}}{h_{m_1b}^{\max}} \cdot \gamma_{m_1b}^{\max} = \left(\frac{d_{m_1b}}{d_{m_1b}^{\min}}\right)^{\eta} \gamma_{m_1b}^{\max},$$

$$\gamma_{m_1m_2} = \frac{h_{m_1m_2}\overline{P_{m_1}}}{N} = \frac{h_{m_2m_2}}{h_{m_1m_2}^{\max}} \cdot \gamma_{m_1m_2}^{\max} = \left(\frac{d_{m_1m_2}}{d_{m_1m_2}^{\min}}\right)^{\eta} \gamma_{m_1m_2}^{\max},$$

$$\gamma_{bm_2} = \frac{h_{bm_2}\overline{P_b}}{N} = \frac{h_{bm_2}}{h_{bm_2}^{\max}} \cdot \gamma_{bm_2}^{\max} = \left(\frac{d_{bm_2}}{d_{bm_2}^{\min}}\right)^{\eta} \gamma_{bm_2}^{\max},$$

where $d_{uv,min}$ is a reference distance at which $\gamma_{uv} = \gamma_{uv}^{\max}$ for $u, v \in \{b, m_1, m_2\}$, $x \neq y$.

For the purpose of comparison, we will assume that $d_{bm_2}^{\min} = d_{m_1b}^{\min} = d_{m_1m_2}^{\min} \equiv d^{\min}$, which would correspond to $\overline{P_b} = \overline{P_m}$, and normalize all distances to $d^{\min}$ (or, equivalently, take $d^{\min} = 1$). Note that by assuming $\overline{P_b} = \overline{P_m}$ we estimate an upper bound on the capacity region extension, since in practice $\overline{P_m} \leq \overline{P_b}$, and from Lemma 6.1 if FD rate can be greater than the maximum TDD rate, it is maximized when the transmission power levels are maximized.

Capacity region extension as a function of SNRs is shown in Fig. 8, for different values of the path loss exponent and $d_{m_1m_2} = \rho(d_{m_1b} + d_{bm_2})$, for $\rho \in \{0.25, 0.5, 0.75, 1\}$. For all combinations of SNRs at which the triangle inequality is not satisfied, we set the capacity region extension p to 0.

Fig. 8 suggests that to achieve over 50% capacity region extension, the environment needs to be sufficiently lossy, i.e., with the path loss exponent $\eta > 2$. Moreover, to achieve high capacity region extension, the SNRs at the BS and at the MS 2 need to be low enough, meaning that the corresponding distances d_{m_1b} and d_{bm_2} need to be large, since the differences in the SNR shown in all the graphs are due to different distances (and consequently different path loss).

7. OFDM BIDIRECTIONAL LINKS

In this section, we focus on the rate maximization for use case (iii) (Fig. 1(c)). Recall that in this use case the FD receiver at the MS has a frequency-selective SIC profile (Fig. 4(d)). Requiring two technical conditions (Conditions 7.2 and 7.4), we derive a nearly optimal algorithm for the sum rate maximization. While the derived algorithm is nearly optimal and has polynomial time complexity, its running time is high because it requires invoking a large number of gradient ascent methods. We therefore also consider a high SINR approximation of the sum rate, and develop an efficient power allocation algorithm for the sum rate maximization. We also prove that in the high SINR regime it is always optimal to set the maximum SIC frequency in the middle of the used frequency band. Interestingly, our numerical results (Section 7.3) suggest that for FD capacity region extension of over 50%, the high SINR approximation provides a solution that is very close to the optimal one.

7.1 Analysis of Sum Rate

7.1.1 Dependence on Channel Power Levels

The analysis of the sum rate in terms of transmission power levels extends from the single-channel case provided in Section 5. In particular:

OBSERVATION 7.1. *If*

$$\frac{g_m(k-c)^2}{N_m} \leq \frac{h_{mb,k}}{N_b + g_b P_{b,k}} \text{ and } \frac{g_b}{N_b} \leq \frac{h_{bm,k}}{N_m + g_m P_{m,k}(k-c)^2} \quad (11)$$

hold, then the sum rate is concave in both $P_{m,k}$ and $P_{b,k}$.

This result is simple to show, since $(k-c)^2$ term is independent of the transmission power levels, and $P_{b,k}$ and $P_{m,k}$ only appear in one summation term (r_k). Therefore, we get the same form of partial derivatives in $P_{b,k}$ and $P_{m,k}$ as in the case of a single channel (proof of Lemma 5.1). Similar to the case of a single channel, if condition (11) is not satisfied, then the achievable rate improvement is low (cf. Prop. 5.4).

The first inequality in (11) guarantees concavity in $P_{m,k}$, while the second one guarantees concavity in $P_{b,k}$. The condition (11) cannot be satisfied for any $P_{b,k} \geq 0$, $P_{m,k} \geq 0$ (e.g., the first inequality cannot be satisfied if $\frac{g_m(k-c)^2}{N_m} > \frac{h_{mb,k}}{N_m}$). However, since the role of condition (11) is to guar-

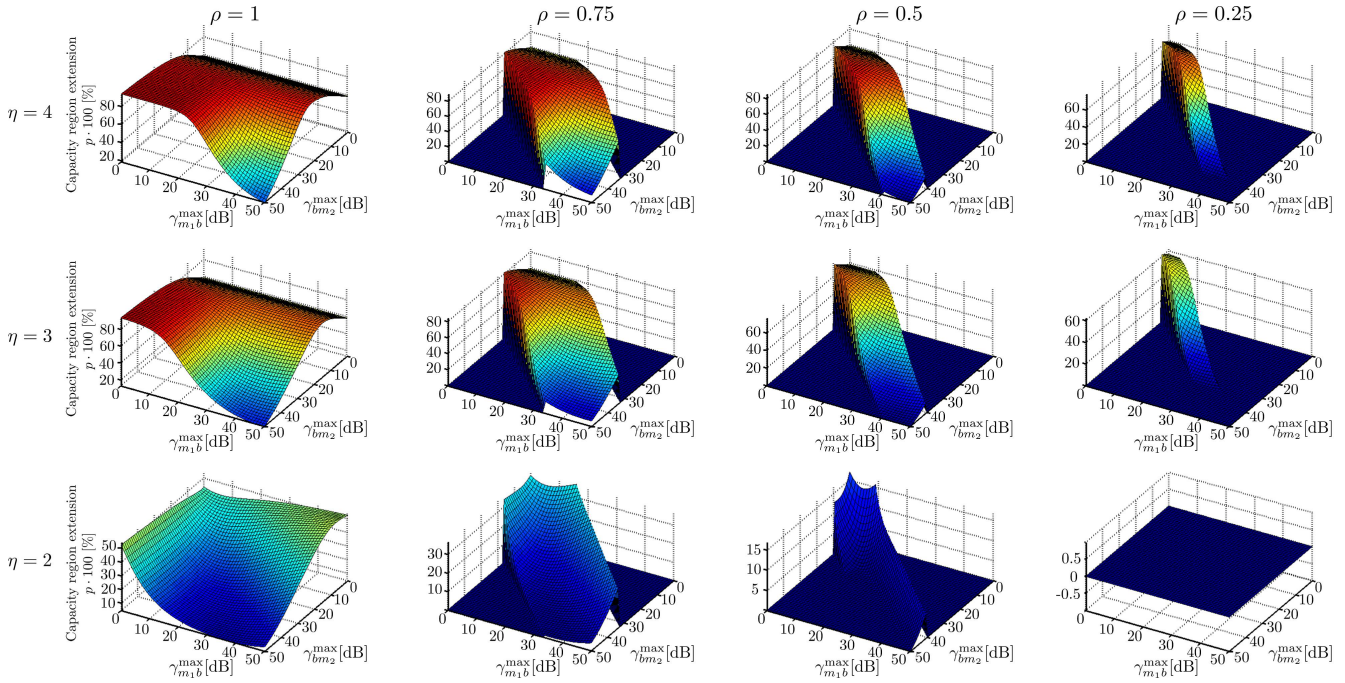

Figure 8: TDD capacity region extension due to FD as a function of SNRs, where SNRs change due to path loss with exponent η, and distance between MS 1 and MS 2 is $d_{m_1m_2} = \rho(d_{m_1b} + d_{bm_2})$. Transmission power levels are set to maximum. In SNR regions where the triangle inequality of the distances is not satisfied, p is set to 0.

antee concavity in the power levels, we can replace this condition by either $P_{m,k} = 0$ or $P_{b,k} = 0$, which implies rate concavity in $P_{m,k}, P_{b,k}$. Specifically, to guarantee that the sum rate is concave in all $P_{m,k}, P_{b,k}$, we require the following condition to hold:

CONDITION 7.2. *(a)* $\frac{g_m(k-c)^2}{N_m} \leq \frac{h_{mb,k}}{N_b + g_b P_{b,k}}$ *if* $\frac{g_m(k-c)^2}{N_m} < \frac{h_{mb,k}}{N_b}$*, otherwise* $P_{m,k} = 0$*, and*
(b) $\frac{g_b}{N_b} \leq \frac{h_{bm,k}}{N_m + g_m P_{m,k}(k-c)^2}$ *if* $\frac{g_b}{N_b} < \frac{h_{bm,k}}{N_m}$*; otherwise* $P_{b,k} = 0$ *if* $P_{m,k}$ *was not set to 0 by (a).*

Note that Condition 7.2 forces a channel k to be used in half-duplex (only one of $P_{m,k}, P_{b,k}$ is non-zero) whenever it is not possible to satisfy the sufficient condition (11) for the sum rate concavity in $P_{m,k}, P_{b,k}$ for any $P_{m,k} \geq 0$ and $P_{b,k} \geq 0$.

7.1.2 Dependence on Maximum SIC Frequency

The following lemma shows that choosing optimal c for a given power allocation $\{P_{b,k}, P_{m,k}\}$ is hard in general, since the sum rate r as a function of c is neither convex nor concave, and can have $\Omega(K)$ local maxima. Proofs of the following two lemmas are provided in [23].

LEMMA 7.3. *The sum rate r is neither convex nor concave in c. All (local) maxima of $r(c)$ lie in the interval $(1, K)$. In general, the number of local maxima is $\Omega(K)$.*

Even though $r(c)$ can have multiple maxima in c, if we restrict the analysis to practically relevant values of $\gamma_{mb,k}$ and $\gamma_{mm,k}$, the selection of c, together with the power allocation, can be made tractable under the following condition:

CONDITION 7.4. $\frac{g_m P_{m,k}}{N_m} \leq \gamma_{mb,k}$ $\forall k \in \{1, ..., K\}$.

Note that this condition is implied by Condition 7.2 for $|k-c| \geq 1$, and that there can be at most 2 channels with $|k-c| < 1$. For $|k-c| < 1$, this condition limits SI on channel k. The following lemma bounds the first partial derivative of r with respect to c. This bound will prove useful in maximizing r as a function of c and $\{P_{b,k}, P_{m,k}\}$ (Section 7.2.1).

LEMMA 7.5. *If Condition 7.4 holds, then:*

$$\left|\frac{\partial r}{\partial c}\right| \leq \frac{2}{\ln 2}(\ln(K) + 1 + 2\sqrt{3}) \quad \forall c \in (1, K).$$

7.2 Parameter Selection Algorithms

7.2.1 General SINR Regime

The pseudocode of the algorithm for maximizing the sum rate in the general SINR regime is provided in Algorithm 1 – MAXIMUMRATE. We claim the following:

LEMMA 7.6. *Under conditions 7.2 and 7.4,* MAXIMUMRATE *determines c and the power allocation $\{P_{b,k}, P_{m,k}\}$ that maximize sum rate up to an absolute error ϵ, for any $\epsilon > 0$. The running time of* MAXIMUMRATE *is polynomial in $\frac{1}{\epsilon}$ and K.*

Note that if Algorithm 1 only applied gradient ascent to maximize the sum rate without requiring Condition 7.2, it would not necessarily obtain an optimal or a near-optimal power allocation. This is because without Condition 7.2 the sum rate is not necessarily concave in the power variables, and gradient ascent methods could converge to a local (instead of global) optimum. Moreover, since the sum rate is highly nonlinear in the parameter c (Lemma 7.3), c cannot be used as a variable in the gradient ascent. Nevertheless,

Algorithm 1 MAXIMUMRATE(ϵ)

Input: $K, \overline{P_b}, \overline{P_m}, g_b, g_m, N_m, N_b$
1: $c_{\min} = 1$, $c_{\max} = K$, $\Delta c = \frac{\epsilon}{\frac{2}{\ln 2}(\ln(K)+1+2\sqrt{3})}$
2: $c^{\max} = r^{\max} = 0$, $\{P_{b,k}^{\max}\} = \{P_{m,k}^{\max}\} = \{0\}$
3: **for** $c = c_{\min}$, $c < c_{\max}$, $c = c + \Delta c$ **do**
4: Solve via gradient ascent:
$\max \quad r = \sum_{k=1}^{K} r_k$, where r_k is given by (5)
s.t. Conditions 7.2 and 7.4 hold
$\sum_{k=1}^{K} P_{m,k} \le \overline{P_m}, \quad \sum_{k=1}^{K} P_{b,k} \le \overline{P_b}$
$P_{b,k} \ge 0, \quad P_{m,k} \ge 0 \quad \forall k \in \{1, ..., K\}$.
5: **if** $r > r^{\max}$ **then**
6: $r^{\max} = r, \quad c^{\max} = c,$
7: $\{P_{b,k}^{\max}\} = \{P_{b,k}\}, \quad \{P_{m,k}^{\max}\} = \{P_{m,k}\}$
8: **return** $c^{\max}, \{P_{b,k}^{\max}\}, \{P_{m,k}^{\max}\}, r^{\max}$.

as a result of Lemma 7.5 that bounds the first derivative of r with respect to c when Condition 7.4 is applied, by examining a sufficient number of choices for c from the interval $(1, K)$ and determining an optimal power allocation for each such c, the algorithm determines a nearly-optimal solution.

PROOF OF LEMMA 7.6. Consider the optimization problem in Step 4 of the algorithm. Since Condition 7.2 is required by the constraints, the objective r is concave in $P_{b,k}, P_{m,k}$. The feasible region of the problem from Step 4 is determined by linear inequalities and Conditions 7.2 and 7.4.

Condition 7.2 is either an inequality or an equality for each $P_{m,k}, P_{b,k}$ that (possibly rearranging the terms) is linear in $P_{m,k}, P_{b,k}$. Condition 7.4 is a linear inequality in $P_{m,k}$. Therefore, the feasible region in the problem of Step 4 is a polyhedron and therefore convex. It follows immediately that this problem can be solved optimally via a gradient ascent method in time polynomial in K.

The algorithm finds an optimal power allocation for each c from the set of $\frac{(K-1)(\frac{2}{\ln 2}(\ln(K)+1+2\sqrt{3}))}{\epsilon} - 2$ equally spaced points from the interval $(1, K)$, and chooses c and power allocation that provide maximum sum rate r.

What remains to prove is that by choosing any alternative $c \neq c^{\max}$ and accompanying optimal power allocation the sum rate cannot be improved by more than an additive ϵ.

Recall from Lemma 7.3 that optimal c must lie in $(1, K)$. Suppose that there exist $c^*, \{P_{b,k}^*, P_{m,k}^*\}$ such that $c^* \in (1, K)$, $c^* \neq c^{\max}$ and $r(c^*, \{P_{b,k}^*, P_{m,k}^*\}) > r^{\max} + \epsilon$.

From the choice of points c in the algorithm, there must exist at least one point c^a that the algorithm considers such that $|c^a - c^*| < \Delta c = \frac{\epsilon}{\frac{2}{\ln 2}(\ln(K)+1+2\sqrt{3})}$. From Lemma 7.5,

$$r(c^*, \{P_{b,k}^*, P_{m,k}^*\}) - r(c^a, \{P_{b,k}^*, P_{m,k}^*\}) < \frac{\epsilon}{\frac{2}{\ln 2}(\ln(K)+1+2\sqrt{3})} \cdot \Big(\frac{2}{\ln 2}(\ln(K)+1+2\sqrt{3})\Big) = \epsilon,$$

since in any finite interval I any continuous and differentiable function $f(x)$ cannot change by more than the length of the interval I times the maximum value of its first derivative $f'(x)$ (a simple corollary of the Mean-Value Theorem).

Since the algorithm finds an optimal power allocation for each c, we have that $r(c^a, \{P_{b,k}^*, P_{m,k}^*\}) \le r(c^a, \{P_{b,k}^a, P_{m,k}^a\}) \le r^{\max}$. Therefore: $r(c^*, \{P_{b,k}^*, P_{m,k}^*\}) - r^{\max} < \epsilon$, which is a contradiction. □

7.2.2 High SINR Regime

A high SINR approximation of the sum rate is:

$$r \approx \sum_{k=1}^{K} \Big(\log\Big(\frac{\gamma_{mb,k}}{1+\gamma_{bb,k}}\Big) + \log\Big(\frac{\gamma_{bm,k}}{1+\gamma_{mm,k}}\Big)\Big). \qquad (12)$$

While in the high SINR regime the dependence of sum rate on each power level $P_{b,k}, P_{m,k}$ for $k \in \{1, ..., K\}$ becomes concave (regardless of whether Condition 7.2 holds or not), the dependence on the parameter c remains neither convex nor concave as long as we consider a general power allocation. Therefore, we cannot derive a closed form expression for c in terms of an arbitrary power allocation. However, as we show in Lemma 7.9, when power allocation and the choice of parameter c are considered jointly, it is always optimal to place c in the middle of the interval $(1, K)$: $c = \frac{K+1}{2}$. The following proposition and lemma characterize the optimal power allocation for a given c.

PROPOSITION 7.7. *Under high-SINR approximation and any power allocation $\{P_{m,k}\}$ at the MS and any choice of c, it is always optimal to allocate BS power levels as $P_{b,k} = \frac{\overline{P_b}}{K}$.*

PROOF. Let P_b denote the total irradiated power by the BS. Write power levels on individual subchannels as $P_{b,k} = \beta_k P_b$, where $\beta_k \ge 0$, $\forall k \in \{1, ..., K\}$, and $\sum_{k=1}^{K} \beta_k = 1$. Then the sum rate can be written as:

$$r = \sum_{k=1}^{K} \Big(\log\Big(\frac{h_{mb,k} P_{m,k}}{N_b + g_b \beta_k P_b}\Big) + \log\Big(\frac{h_{bm,k} \beta_k P_b}{N_m + g_m (k-c)^2 P_{m,k}}\Big)\Big).$$

First, observe that

$$\frac{\partial r}{\partial P_b} = \sum_{k=1}^{K} \mathbb{1}_{\{\beta_k > 0\}} \left(\frac{1}{P_b} - \frac{g_b \beta_k}{N_b + g_b \beta_k P_b}\right) = \sum_{k=1}^{K} \mathbb{1}_{\{\beta_k > 0\}} \Big({P_b}^{-1} - (N_b/(g_b \beta_k) + P_b)^{-1} \Big),$$

where $\mathbb{1}_{\{.\}}$ is an indicator function. Since $\beta_k \ge 0$ $\forall k \in \{1, ..., K\}$ and $\sum_{k=1}^{K} \beta_k = 1$, it follows that there exists at least one strictly positive β_k. For each such β_k, $\mathbb{1}_{\beta_k > 0} \Big(\frac{1}{P_b} - \frac{1}{\frac{N_b}{g_b \beta_k} + P_b} \Big) > 0$, since $P_b < \frac{N_b}{g_b \beta_k} + P_b$. Therefore, $\frac{\partial r}{\partial P_b} > 0$, which implies that it is optimal to choose $P_b = \overline{P_b}$.

Taking the first and the second partial derivative of r with respect to each β_k, it is simple to show that r has the same dependence on each β_k, and, moreover, is strictly concave in each β_k, as $\frac{\partial^2 r}{\partial {\beta_k}^2} = -\frac{1}{{\beta_k}^2} + \frac{1}{\left(\frac{N_b}{g_b P_b} + \beta_k\right)^2} < 0$, where the inequality follows from $\beta_k < \frac{N_b}{g_b P_b} + \beta_k$. Therefore, r is maximized for $\beta_k = \frac{1}{K}$. □

LEMMA 7.8. *Under high-SINR approximation and for a fixed c, the optimal power allocation at the MS satisfies $P_{m,k} = \alpha_k \cdot \overline{P_m}$, where $\alpha_k \ge 0$, $\sum \alpha_k = 1$, and for $k \neq K$:*
(i) $\alpha_k = \Big(\frac{1}{\alpha_K} - \frac{1}{N_m / R_K + \alpha_K}\Big)^{-1}$ *if* $k = c$,
(ii) $\alpha_k = \frac{-N_m + \sqrt{{N_m}^2 + 4\alpha_K (N_m + R_K \alpha_K) R_k}}{2R_k}$ *if* $k \neq c$,
where $R_k = g_m (k-c)^2 P_m$ *for* $k \in \{1, ..., K\}$.

PROOF. Let $P_{m,k} = \alpha_k \cdot P_m$, where $\alpha_k > 0$, $\forall k$, and $\sum_{k=1}^{K} \alpha_k = 1$. The sum rate can then be written as:

$$r = \sum_{k=1}^{K} \Big(\log\Big(\frac{h_{mb,k}\alpha_k P_m}{N_b + g_b P_{b,k}}\Big) + \log\Big(\frac{h_{bm,k}P_{b,k}}{N_m + g_m(k-c)^2\alpha_k P_m}\Big)\Big).$$

Proving that at the optimal solution that maximizes r we necessarily have $P_m = \overline{P_m}$ is analogous to the proof given in Proposition 7.7 for $P_b = \overline{P_b}$, and it is therefore omitted.

As $\sum_{k=1}^{K} \alpha_k = 1$, only $K-1$ α_k's can be chosen independently, while the value of the remaining one is implied by their sum being equal to 1. Choose $\alpha_K = 1 - \sum_{k=1}^{K-1} \alpha_k$, and observe that that $K - c \neq 0$ (and therefore $R_K \neq 0$) is always true since, similar as in the proof of Lemma 7.3, at the optimum it must be $c \in (1, K)$.

If $R_k = g_m(k-c)^2 P_m = 0$, then the first and the second derivative of r with respect to α_k are given as:

$$\begin{aligned}\frac{\partial r}{\partial \alpha_k} &= \frac{1}{\alpha_k} + \frac{1}{\alpha_K}\frac{\partial \alpha_K}{\partial \alpha_k} - \frac{R_K}{N_m + R_K\alpha_K}\frac{\partial \alpha_K}{\partial \alpha_k} \\ &= \frac{1}{\alpha_k} - \frac{1}{\alpha_K} + \frac{R_K}{N_m + R_K\alpha_K}, \\ \frac{\partial^2 r}{\partial {\alpha_k}^2} &= -\frac{1}{\alpha_k^2} - \left(\frac{1}{\alpha_K^2} - \frac{{R_K}^2}{(N_m + R_K\alpha_K)^2}\right) \\ &= -\frac{1}{\alpha_k^2} - \left(\frac{1}{\alpha_K^2} - \frac{1}{(N_m/R_K + \alpha_K)^2}\right) < 0.\end{aligned}$$

It follows that r is concave in α_k and maximized for

$$\alpha_k = \left({\alpha_K}^{-1} - (N_m/R_K + \alpha_K)^{-1}\right)^{-1}, \quad (13)$$

where $R_K = g_m(K-c)^2 P_m$.

If $R_k \neq 0$, then the first and the second derivative are:

$$\begin{aligned}\frac{\partial r}{\partial \alpha_k} &= \frac{1}{\alpha_k} - \frac{R_k}{N_i + R_k\alpha_k} - \frac{1}{\alpha_K} + \frac{R_K}{N_m + R_K\alpha_K}, \\ \frac{\partial^2 r}{\partial {\alpha_k}^2} &= -\frac{1}{\alpha_k^2} + \frac{{R_k}^2}{(N_m + R_k\alpha_k)^2} - \frac{1}{\alpha_K^2} + \frac{{R_K}^2}{(N_m + R_K\alpha_K)^2} \\ &= -\left({\alpha_k}^{-2} - (N_m/R_k + \alpha_k)^{-2}\right) \\ &\quad -\left({\alpha_K}^{-2} - (N_m/R_k + \alpha_K)^{-2}\right) < 0.\end{aligned}$$

It follows that r is concave in α_k and maximized for:

$$\frac{\partial r}{\partial \alpha_k} = \frac{1}{\alpha_k} - \frac{R_k}{N_i + R_k\alpha_k} - \frac{1}{\alpha_K} + \frac{R_K}{N_m + R_K\alpha_K} = 0. \quad (14)$$

After simplifying (14), we get:

$$\alpha_k(N_m + R_k\alpha_k) = \alpha_K(N_m + R_K\alpha_K). \quad (15)$$

Solving the quadratic equation (15) for α_k and using that $\alpha_k > 0$, it follows that r is maximized when α_k satisfies

$$\alpha_k = \frac{-N_m + \sqrt{{N_m}^2 + 4\alpha_K(N_m + R_K\alpha_K)R_k}}{2R_k}, \quad (16)$$

where $R_k = g_m(k-c)^2 P_m$. □

It is relatively simple to show (using similar approach as in the proof of Lemma 7.3) that under general power allocation r can have up to K local maxima with respect to c. However, if c is considered jointly with the optimal power allocation corresponding to c (Proposition 7.7 and Lemma 7.8), it is always optimal to place c in the middle of the interval $(1, K)$, as the following lemma states.

LEMMA 7.9. *If $(c, \{P_{b,k}, P_{m,k}\})$ maximizes the sum rate under high SINR approximation, then $c = \frac{K+1}{2}$.*

Even though this result may seem intuitive because the optimal power allocation is always symmetric around c (Proposition 7.7 and Lemma 7.8), the proof does not follow directly from this property and requires many technical details. For this reason, the proof is provided in [23].

A simple corollary of Lemma 7.9 is that:

COROLLARY 7.10. *If $(c^*, \{P_{m,k}^{\max}, P_{b,k}^{\max}\})$ maximizes r under high SINR approximation, then the power allocation $\{P_{m,k}^{\max}\}$ is symmetric around $\frac{K+1}{2}$ and decreasing in $|k-c|$.*

PROOF. The first part follows directly from $c^{\max} = \frac{K+1}{2}$. The proof of the second part can be found in [23] (proof of Lemma 7.9, Claim (K2)). □

LEMMA 7.11. *A solution $(c^{\max}, \{P_{m,k}^{\max}, P_{b,k}^{\max}\})$ that maximizes r under high SINR approximation up to an absolute error ϵ can be computed in $O\left(K \log\left(\frac{1}{\epsilon}\right)\right)$ time.*

PROOF. From Proposition 7.7, at the optimum $P_{b,k}^{\max} = \frac{P_{b,\max}}{K}$, $\forall k \in \{1, ..., K\}$. This can be computed in constant time, and requires $\Theta(K)$ time to assign the values to all the $P_{b,k}$'s. From Lemma 7.9, $c^{\max} = \frac{K+1}{2}$.

From Lemma 7.8, $P_{m,k}^{\max} = \alpha_k \cdot \overline{P_m}$, where $\{\alpha_k\}$ are positive coefficients given by (13), (16) and $\sum_{k=1}^{K} \alpha_k = 1$. Recall that all the α_k's are given in terms of α_K, so we can determine the allocation $\{\alpha_k\}$ by performing a binary search for α_K until $\sum_{k=1}^{K} \alpha_k \in [1-\epsilon', 1]$. Corollary 7.10 implies that $\alpha_K \leq \frac{1}{K}$, so it is sufficient to perform the binary search for α_K only within the interval $\left[0, \frac{1}{K}\right]$. Such binary search requires $O\left(\log\left(\frac{1}{K\epsilon'}\right)\right)$ iterations, with each iteration requiring $O(K)$ time to compute $\{\alpha_k\}$ and evaluate $\sum_{k=1}^{K} \alpha_k$, for the total time $O\left(K \log\left(\frac{1}{K\epsilon'}\right)\right)$.

The last part of the proof is determining an appropriate ϵ' so that $r(c^{\max}, \{P_{m,k}^{\max}, P_{b,k}^{\max}\}) \geq \max r - \epsilon$, where the maximum is taken over all feasible points $(c, \{P_{m,k}, P_{b,k}\})$. Notice that we are only deviating from the optimal solution in that $\sum_{k=1}^{K} P_{m,k}^{\max} = \overline{P_m} \cdot \sum_{k=1}^{K} \alpha_k \in [\overline{P_m}(1-\epsilon'), \overline{P_m}]$ instead of $\sum_{k=1}^{K} P_{m,k}^{\max} = \overline{P_m}$. Therefore, $(c^{\max}, \{P_{m,k}^{\max}, P_{b,k}^{\max}\})$ is the optimal solution to the problem that is equivalent to the original problem, with maximum total power at the MS equal to $\overline{P_m} \cdot \sum_{k=1}^{K} \alpha_k$. Observe that:

$$\frac{\partial r}{\partial P_m} = \sum_{k=1}^{K} \Big(\frac{1}{P_m} - \frac{1}{\frac{N_m}{g_m(k-c)^2} + P_i} \cdot \mathbb{1}_{\{k \neq c\}}\Big) \leq \frac{K}{P_m}.$$

As $\frac{\partial r}{\partial P_m}(P_m) \leq \frac{K}{\overline{P_m}(1-\epsilon')}$ for $P_m \in [\overline{P_m}(1-\epsilon'), \overline{P_m}]$, it follows that: $\max r - r(c^{\max}, \{P_{m,k}^{\max}, P_{b,k}^{\max}\}) \leq \frac{K}{\overline{P_m}(1-\epsilon')} \cdot \overline{P_m}\epsilon'$. Setting: $\frac{K}{\overline{P_m}(1-\epsilon')} \cdot \overline{P_m}\epsilon' = \epsilon \quad \Leftrightarrow \quad \epsilon' = \frac{\epsilon}{K+\epsilon}$, we yield the total running time of: $O\left(K \log\left(\frac{K+\epsilon}{K\epsilon}\right)\right) = O\left(K \log\left(\frac{1}{\epsilon}\right)\right)$. □

We summarize the results from this section in Algorithm 2 – HSINR-MAXIMUMRATE.

7.3 Measurement-based Numerical Evaluation

This section presents numerical evaluations for use case (iii). Numerical evaluations for use cases (i) and (ii) were already provided in Sections 5 and 6, respectively.

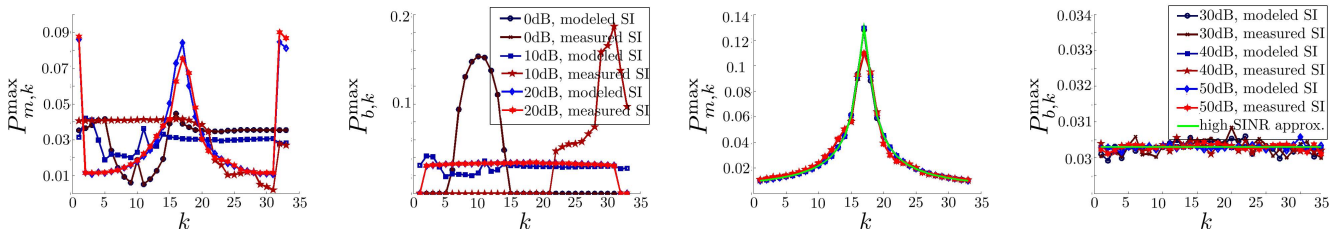

Figure 9: Power allocation over channels for SNR (a), (b) 0dB–20dB and (c), (d) 30dB–50dB. The graphs show the results obtained by running MaximumRate with measured SI and modeled SI at the input. Graphs (c) and (d) also show the power allocation computed by HSINR-MaximumRate. For SNR $\geq$ 30dB all three power allocations match closely.

Algorithm 2 HSINR-MaximumRate(ϵ)

Input: $K, \overline{P_b}, \overline{P_m}, g_b, g_m, N_m, N_b$
1: $c^{\max} = (K+1)/2$
2: $\{P^{\max}_{b,k}\} = \overline{P_b}/K$, $\forall k \in \{1, ..., K\}$
3: **for** $\alpha_K \in [0, 1/K]$, via a binary search **do**
4: Compute α_k for $1 \leq k \leq K-1$ using (13) and (16)
5: End binary search when $\sum_{k=1}^{K} \alpha_k \in [1-\epsilon/(K+\epsilon), 1]$
6: **return** $c^{\max}, \{P^{\max}_{b,k}\}, \{P^{\max}_{m,k}\}$.

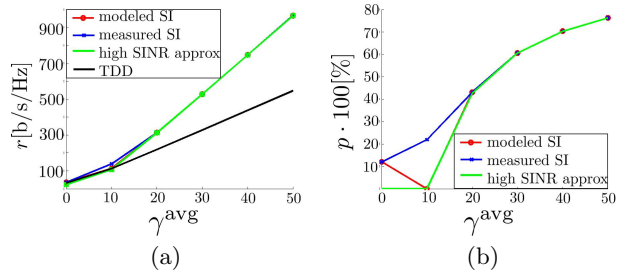

Figure 10: Evaluated (a) sum rate and (b) capacity region extension as a function of $\gamma^{\text{avg}} = \frac{h_{bm,k}\frac{1}{K}}{N_m} = \frac{h_{mb,k}\frac{1}{K}}{N_b}$. For $\gamma^{\text{avg}} \geq$ 20dB, sum rate and capacity region extension obtained from MaximumRate (both with measured and modeled SI profile) and HSINR-MaximumRate match closely.

We focus on the impact of a frequency-selective SIC profile in a small form factor hardware at the MS (Fig. 4(d)), and evaluate rate gains based on measurements and the model presented in Sections 3 and 4.1, respectively.

To determine the position $c^{\max}$ of maximum SIC and the power allocation $\{P^{\max}_{m,k}, P^{\max}_{b,k}\}$ that maximize the sum rate, we run an implementation of the MaximumRate algorithm separately for measured ([32,34] and Fig. 4(d)) and modeled (Eq. (1)) SIC profiles of the MS FD receiver. Additionally, we determine $c^{\max}, \{P^{\max}_{m,k}, P^{\max}_{b,k}\}$ for the high SINR approximation of the sum rate using HSINR-MaximumRate.

Since the measurements were performed only for the analog part of the FD receiver, we assume additional 50dB of cancellation from the digital domain.[4] Similar to [5], we assume that when either station transmits at maximum total power that is equally allocated across channels (so that $P_{m,k} = \frac{\overline{P_m}}{K}, P_{b,k} = \frac{\overline{P_b}}{K}$), the noise on each channel is 110dB below the transmitted power level.

[4]Note that Fig. 4(d) only shows isolation that results from the SIC in the analog domain.

We consider a total bandwidth of 20MHz in the range 2.13–2.15GHz, and take the distance between the measurement points as the OFDM channel width ($\approx$ 600kHz), so that there are $K = 33$ channels in the considered band. For the SIC at the BS, we take $g_b = 1$ [5].

We scale all the power variables so that $\overline{P_m} = \overline{P_b} = 1$, and normalize the SNR to the scaled values of power levels on channels. We consider flat frequency fading, and perform numerical evaluations for $\frac{h_{mb,k}}{N_b} = \frac{h_{bm,k}}{N_m} \equiv \gamma^{\text{avg}} \cdot K$, $\forall k$, where $\gamma^{\text{avg}} \in \{0, 10, 20, 30, 40, 50\}$ [dB].

We run MaximumRate for $\Delta c = 0.01$, which translates into an absolute error $\epsilon \approx 0.2$ for r. We evaluate the sum rate and the capacity region extension using the measurement data for the remaining SI and $c^{\max}, \{P^{\max}_{m,k}, P^{\max}_{b,k}\}$ returned by the algorithm. We assume that the SIC profile does not change as f_c (and correspondingly c) is varied. To run the algorithm for c positioned at any point between two neighboring channels, we interpolate the measurement data.

Since for the transmitted power of $1/K$ and c placed in the middle of the frequency band XINR at the first and the last channel is about 35 ($\approx$ 15dB), our numerical results suggest, as expected (see e.g., Fig. 5(b) and Fig. 6(b)), that to achieve high rate gain, γ^{avg} needs to be sufficiently high.

Fig. 9(a) and 9(b) show the power allocation at the MS and at the BS computed by MaximumRate for $\gamma^{\text{avg}} \in \{0, 10, 20\}$[dB] for measured and modeled SI. For γ^{avg} up to 10dB the algorithm selects most of the channels as half-duplex, where either $P^{\max}_{m,k} = 0$ or $P^{\max}_{b,k} = 0$. At $\gamma^{\text{avg}} =$ 20dB, all except for three channels at the edges of the frequency band are operating in FD.

Fig. 9(c) and 9(d) show the power allocation at the MS and at the BS computed by the MaximumRate algorithm for $\gamma^{\text{avg}} \in \{30, 40, 50\}$[dB] for the measured and modeled SI, and computed by the HSINR-MaximumRate algorithm for the high SINR approximation of the sum rate. In all the cases $\gamma^{\text{avg}} \in \{30, 40, 50\}$[dB] the power allocations returned by the algorithms for the measured and modeled SI and for the high SINR approximation of the sum rate match closely.

Fig. 10(a) shows the rate as a function of average SNR for $c_{\max}, \{P^{\max}_{m,k}, P^{\max}_{b,k}\}$ returned by the MaximumRate algorithm for the measured and modeled SI and returned by the HSINR-MaximumRate algorithm. Fig. 10(a) also shows the maximum TDD rate as a function of the average SNR. Fig. 10(b) shows the capacity region extension for $c_{\max}, \{P^{\max}_{m,k}, P^{\max}_{b,k}\}$ determined by the MaximumRate algorithm for the measured and modeled SI, and computed using the HSINR-MaximumRate algorithm. As suggested by Fig. 10(a) and 10(b), for low average SNR, mainly for

$\gamma^{\text{avg}} \leq 10$dB, the achievable rate improvements are low; in particular, capacity region extension is up to about 20%. (Recall from Fig. 9(a) and 9(b) that in that case most channels are selected as half-duplex by the MaximumRate.) For $\gamma^{\text{avg}} \geq 20$dB, when the power allocation is close to the high SINR approximation (see Fig. 9), more significant rate improvements are observed. In particular, for $\gamma^{\text{avg}} \geq 20$dB the capacity region extension is between 40% and 80%.

8. CONCLUSION AND FUTURE WORK

In this paper we considered three basic use cases of FD, including single- and multi-channel scenarios. In order to analyze the multi-channel scenario, we developed a new model that is grounded in realistic FD receiver implementations for small form factor devices. We characterized the rate gains in different scenarios and solved power allocation and frequency selection problems either analytically or algorithmically. Our numerical results demonstrate the gains from FD in scenarios and for receiver models that have not been studied before.

This is one of the first steps towards understanding the benefits and the complexities associated with FD. Hence, there are still many open problems to consider. In particular, SIC that has different impacts on different channels calls for the design of algorithms for OFDM networks with multiple access and MSs modeled as small form-factor devices. Moreover, we plan to develop scheduling algorithms that support the co-existence of half- and full-duplex users. While significant attention has been given to scheduling and resource allocation in half duplex OFDM networks [6,16], as demonstrated in this paper, the special characteristics of FD pose new challenges that have not been addressed.

9. ACKNOWLEDGEMENTS

This research was supported in part by the NSF grant CNS-10-54856, DARPA RF-FPGA program HR0011-12-1-0006, and the People Programme (Marie Curie Actions) of the European Union's Seventh Framework Programme (FP7/2007-2013) under REA grant agreement n°[PIIF-GA-2013-629740].11.

10. REFERENCES

[1] Skyfr-000709 miniature 2110-2170MHz single junction robust lead circulator data sheet.

[2] E. Ahmed, A. M. Eltawil, and A. Sabharwal. Rate gain region and design tradeoffs for full-duplex wireless communications. *IEEE Trans. Wireless Commun.*, 12(7):3556–3565, July 2013.

[3] E. Aryafar, M. A. Khojastepour, K. Sundaresan, S. Rangarajan, and M. Chiang. MIDU: enabling MIMO full duplex. In *Proc. ACM MobiCom'12*, 2012.

[4] J. Bai and A. Sabharwal. Distributed full-duplex via wireless side-channels: Bounds and protocols. *IEEE Trans. Wireless Commun.*, 12(8):4162–4173, Aug. 2013.

[5] D. Bharadia, E. McMilin, and S. Katti. Full duplex radios. In *Proc. ACM SIGCOMM'13*, 2013.

[6] S. C. Borst, M. G. Markakis, and I. Saniee. Distributed power allocation and user assignment in OFDMA cellular networks. In *IEEE Allerton'11*, 2011.

[7] W. Cheng, X. Zhang, and H. Zhang. Optimal dynamic power control for full-duplex bidirectional-channel based wireless networks. In *Proc. IEEE INFOCOM'13*, 2013.

[8] J. Choi, S. Hong, M. Jain, S. Katti, P. Levis, and J. Mehlman. Beyond full duplex wireless. In *Proc. IEEE Asilomar'12*, 2012.

[9] J. Choi, M. Jain, K. Srinivasan, P. Levis, and S. Katti. Achieving single channel, full duplex wireless communication. In *Proc. ACM MobiCom'10*, 2010.

[10] B. Debaillie, D.-J. van den Broek, C. Lavin, B. van Liempd, E. Klumperink, C. Palacios, J. Craninckx, B. Nauta, and A. Parssinen. Analog/RF solutions enabling compact full-duplex radios. *IEEE J. Sel. Areas Commun.*, 32(9):1662–1673, Sept 2014.

[11] M. Duarte, C. Dick, and A. Sabharwal. Experiment-driven characterization of full-duplex wireless systems. *IEEE Trans. Wireless Commun.*, 11(12):4296–4307, Dec. 2012.

[12] M. Duarte and A. Sabharwal. Full-duplex wireless communications using off-the-shelf radios: Feasibility and first results. In *Proc. IEEE Asilomar'10*, 2010.

[13] M. Duarte, A. Sabharwal, V. Aggarwal, R. Jana, K. Ramakrishnan, C. Rice, and N. Shankaranarayanan. Design and characterization of a full-duplex multiantenna system for WiFi networks. *IEEE Trans. Veh. Technol.*, 63(3):1160–1177, Mar. 2014.

[14] E. Everett, A. Sahai, and A. Sabharwal. Passive self interference suppression for full-duplex infrastructure nodes. *IEEE Trans. Wireless Commun.*, 13(2):680–694, Feb. 2014.

[15] S. Goyal, P. Liu, S. Panwar, R. DiFazio, R. Yang, J. Li, and E. Bala. Improving small cell capacity with common-carrier full duplex radios. In *Proc. IEEE ICC'14*, 2014.

[16] J. Huang, V. G. Subramanian, R. Agrawal, and R. A. B. . Downlink scheduling and resource allocation for OFDM systems. *IEEE Trans. Wireless Commun.*, 8(1):288–296, Jan. 2009.

[17] M. Jain, J. Choi, T. Kim, D. Bharadia, S. Seth, K. Srinivasan, P. Levis, S. Katti, and P. Sinha. Practical, real-time, full duplex wireless. In *Proc. ACM MobiCom'11*, 2011.

[18] A. Khandani. Two-way (true full-duplex) wireless. In *Proc. CWIT'13*, 2013.

[19] M. Khojastepour and S. Rangarajan. Wideband digital cancellation for full-duplex communications. In *Proc. IEEE Asilomar'12*, 2012.

[20] M. Khojastepour, K. Sundaresan, S. Rangarajan, X. Zhang, and S. Barghi. The case for antenna cancellation for scalable full-duplex wireless communications. In *Proc. ACM HotNets'11*, 2011.

[21] M. E. Knox. Single antenna full duplex communications using a common carrier. In *Proc. IEEE WAMICON'12*, 2012.

[22] W. Li, J. Lilleberg, and K. Rikkinen. On rate region analysis of half-and full-duplex OFDM communication links. *IEEE J. Sel. Areas Commun.*, 32(9):1688–1698, Sept. 2014.

[23] J. Marašević, J. Zhou, H. Krishnaswamy, Y. Zhong, and G. Zussman. Resource allocation and rate gains in practical full-duplex systems, Mar. 2015. arXiv preprint, http://arxiv.org/abs/1503.08237.

[24] J. McMichael and K. Kolodziej. Optimal tuning of analog self-interference cancellers for full-duplex wireless communication. In *IEEE Allerton'12*, 2012.

[25] T. S. Rappaport. *Wireless communications: principles and practice*, chapter 4. Prentice-Hall, 2 edition, 2002.

[26] A. Sabharwal, P. Schniter, D. Guo, D. Bliss, S. Rangarajan, and R. Wichman. In-band full-duplex wireless: Challenges and opportunities. *IEEE J. Sel. Areas Commun.*, 32(9):1637–1652, Sept. 2014.

[27] A. Sahai, S. Diggavi, and A. Sabharwal. On uplink/downlink full-duplex networks. In *Proc. IEEE Asilomar'13*, 2013.

[28] A. Sahai, G. Patel, C. Dick, and A. Sabharwal. Understanding the impact of phase noise on active cancellation in wireless full-duplex. In *IEEE Asilomar'12*, 2012.

[29] A. Sahai, G. Patel, and A. Sabharwal. Pushing the limits of full-duplex: Design and real-time implementation. *arXiv preprint arXiv:1107.0607*, 2011.

[30] N. Singh, D. Gunawardena, A. Proutiere, B. Radunovic, H. V. Balan, and P. Key. Efficient and fair MAC for wireless networks with self-interference cancellation. In *Proc. WiOpt'11*, 2011.

[31] X. Xie and X. Zhang. Does full-duplex double the capacity of wireless networks? In *Proc. IEEE INFOCOM'14*, 2014.

[32] J. Zhou, A. Chakrabarti, P. Kinget, and H. Krishnaswamy. Low-noise active cancellation of transmitter leakage and transmitter noise in broadband wireless receivers for FDD/co-existence. *IEEE J. Solid-State Circuits*, 49(12):1–17, Dec. 2014.

[33] J. Zhou, T.-H. Chuang, T. Dinc, and H. Krishnaswamy. A receiver with reconfigurable self-interference cancellation based on RF frequency-domain equalization supporting >20MHz cancellation bandwidth for FDD, co-existence and same-channel full duplex applications. In *Proc. IEEE ISSCC'15*, 2015.

[34] J. Zhou, P. R. Kinget, and H. Krishnaswamy. A blocker-resilient wideband receiver with low-noise active two-point cancellation of >0dBm TX leakage and TX noise in RX band for FDD/co-existence. In *Proc. IEEE ISSCC'14*, 2014.